Spin-canting-driven triple coupling of spin, electric, and valley polarization in two-dimensional antiferromagnetic semiconductors

Chao Liu,[1] Guo-dong Zhao,[2] Silvia Picozzi,[3] Xingxing Li,[1,4,5,*] and Jinlong Yang[1,4,5,†]

[1]*Hefei National Research Center for Physical Sciences at the Microscale, University of Science and Technology of China, Hefei, Anhui 230026, China*

[2]*School of Microelectronics, Fudan University, Shanghai 200433, China*

[3]*Consiglio Nazionale delle Ricerche (CNR-SPIN), Unità di Ricerca presso Terzo di Chieti, c/o Università G. D'Annunzio, I-66100 Chieti, Italy*

[4]*Hefei National Laboratory, University of Science and Technology of China, Hefei, Anhui 230088, China*

[5]*Key Laboratory of Precision and Intelligent Chemistry, University of Science and Technology of China, Hefei, Anhui 230026, China*

(Received 19 December 2023; revised 10 July 2024; accepted 22 August 2024; published 5 September 2024)

Antiferromagnets have aroused widespread interest in spintronics due to negligible stray field and ultrafast spin dynamics. However, antiferromagnets are usually difficult to exhibit the versatile functional properties featured by ferromagnetic materials, particularly the multiple coupling effect among spin, charge, and orbital. Here, based on first-principles calculations, we propose that by exploiting magnetic-field-induced spin canting, the triple coupling of spin, electric, and valley polarization in antiferromagnetic semiconductors can be easily achieved. Taking the two-dimensional (2D) antiferromagnetic semiconductors $MnPS_3$ and $MnPSe_3$ as examples, we demonstrate the occurrence of ferroelectricity and magnetization driven by different canted-antiferromagnetic orders, and their controllability by both electric and magnetic fields. Remarkably, spin canting further results in bipolar magnetic semiconductor properties with reversible spin polarization and valley polarization in valence and conduction bands. Moreover, we illustrate that such spin-driven multiferroics is derived from the subtle interaction of lattice and spin order. This work paves the way to explore magnetoelectric coupling and valley polarization in 2D antiferromagnetic semiconductors.

DOI: 10.1103/PhysRevB.110.094409

Since the discovery of CrI_3 and $Cr_2Ge_2Te_6$ monolayer with long-range magnetic order, the study of two-dimensional (2D) magnetic materials has made significant progress. Ferromagnets have been extensively studied, whereas the exploration of antiferromagnets is relatively insufficient. Antiferromagnetic systems are manifestations of magnetic orders with two coupled magnetic sublattices arranged in such a way that the whole lattice exhibits no macroscopic magnetization [1]. Compared with ferromagnets, antiferromagnets are more common and significantly abundant in nature [2]. Furthermore, due to the ultrafast spin dynamics and zero residual magnetic field, antiferromagnets have drawn great interest in the development of ultrafast and ultrahigh-density spintronics devices such as magnetic memories [3–6]. However, antiferromagnetic systems encounter obstacles in enhancing and extending their functions, mainly owing to the difficulty in achieving efficient tuning and multiple coupling of spin, charge, and orbital degrees [7,8].

Most antiferromagnetic materials exhibit intrinsic collinear spin moments. Applying external physical fields is an effective scheme to tune their magnetic properties [9–12]. For instance, when a magnetic field perpendicular to the direction of the spin order is applied, the local magnetic moment will rotate and produce a spin component in the magnetic field direction, leading to a noncollinear spin-canting configuration [13–16]. Such noncollinear spin structure is usually required for magnetoferroelectric phenomena; for example, materials with intrinsic antiferromagnetic spin-helix and triangular spin frustrated structures are typical type-II multiferroics with strong magnetoelectric coupling [17–21]. In two dimensions, there are a number of antiferromagnetic candidates that can be designed into spin-canting configurations via external fields, providing a great opportunity for enhancing and extending their functions.

In this work, based on first-principles calculations, we achieve triple coupling of spin, electric, and valley polarization in two-dimensional antiferromagnetic semiconductors $MnPX_3$ (X = S, Se) via spin canting. The effect of spin canting on the intensity and direction of resultant electric polarization is clarified. Moreover, the symmetry analysis indicates that spin-canting-driven multiferroics requires combining atomic arrangement and spin ordering to break the spatial inversion symmetry. Furthermore, we show that the spin-canting configuration induces and modulates valley polarization in momentum space. At the same time, a net but opposite spin polarization emerges in the valence and conduction bands, respectively, leading to a bipolar magnetic semiconducting behavior.

Spin-canting-induced ferroelectricity. Hexagonal $MnPS_3$ and $MnPSe_3$ exhibit the Néel-type magnetic structure where the spins of neighboring magnetic atoms are opposite with an in-plane magnetic easy axis [22,23]. By applying a

*Contact author: lixx@ustc.edu.cn
†Contact author: jlyang@ustc.edu.cn

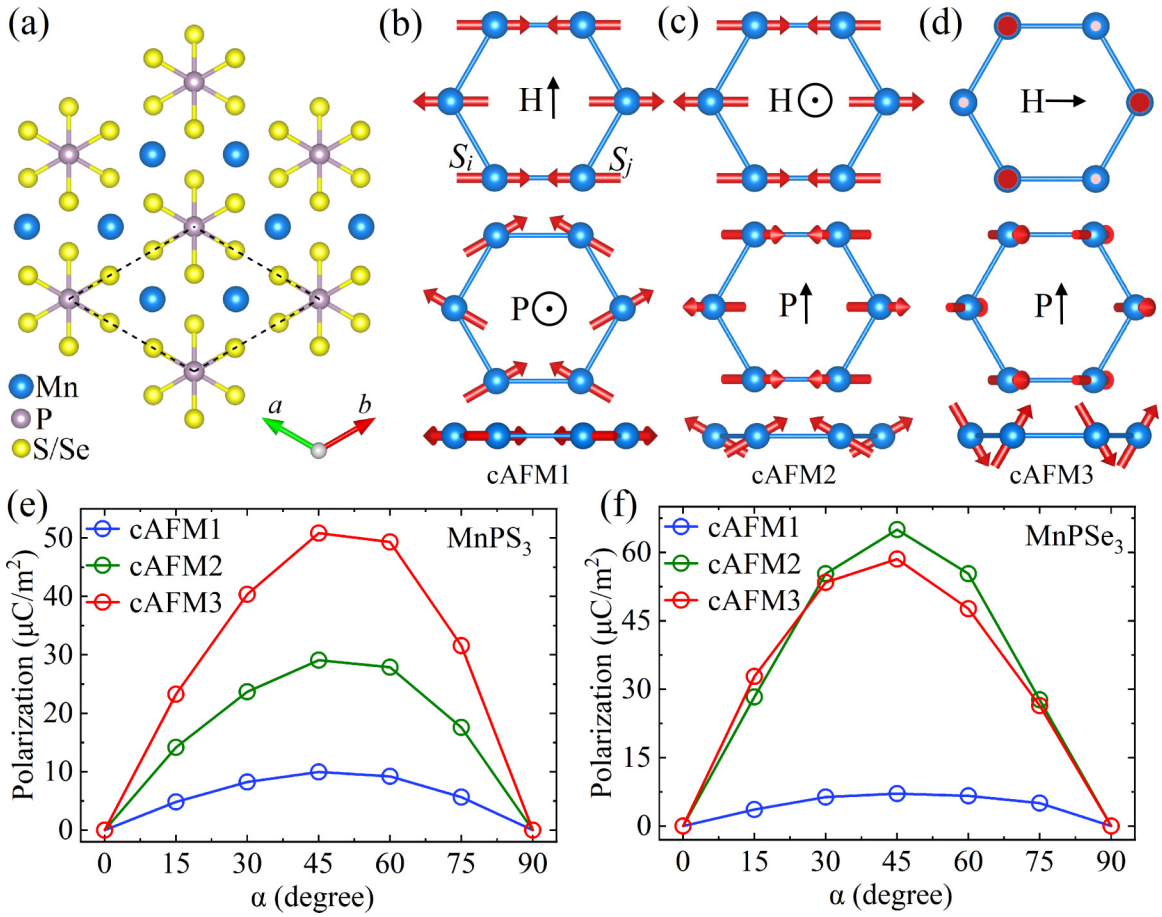

FIG. 1. (a) Top view of the crystal structure of monolayer $MnPX_3$ (X = S, Se). [(b)–(d)] Different initial collinear antiferromagnetic orders and applied magnetic fields H (top) produce three typical spin-canting configurations with different electric polarization P (middle and bottom). [(e), (f)] Spin-canting-induced electric polarization as a function of the spin-canting angle for $MnPS_3$ and $MnPSe_3$ monolayers. The α donates as the angle between the canted spin and its initial direction.

magnetic field perpendicular to the direction of the magnetic moment, the magnetic moment will deflect to the direction of the magnetic field, resulting in a spin tilt. Depending on different directions of initial magnetic moment and applied magnetic field, we classify three typical spin-canting cases as shown in Fig. 1, and designate them as cAFM1 [both the initial magnetic moment and the external magnetic field are in plane; see Fig. 1(b)], cAFM2 [the initial magnetic moment is in plane, while the magnetic field is out of plane; see Fig. 1(c)], and cAFM3 [the initial magnetic moment is out of plane, while the magnetic field is in plane; see Fig. 1(d)]. Additionally, we explore the intertransition between the three spin-canting configurations, and show that the transformation between these three states can be easily realized, as shown in Fig. S1 in the Supplemental Material [24]. Besides, to estimate the magnetic field strength that is needed to induce significant spin canting, Monte Carlo simulations under certain magnetic fields are performed. The results indicate that the antiferromagnetic spin-canting configuration can be achieved by applying an experimentally accessible steady magnetic field; e.g., a steady magnetic field with a strength of 30 T can result in a spin-tilt angle α of approximately 27°. The results are shown in Figs. S2–S4 of the Supplemental Material [24].

In these noncollinear spin structures, the adjacent spin interaction is changed from the original $S_i \cdot S_j$ to include the cross-product part ($S_i \times S_j$). The cross-product term is the expression of the antisymmetric spin-exchange interactions. Such spin interaction combined with the spin-orbit coupling is expected to asymmetrically change the electron charge distribution, inducing an electric dipole moment [46–48]. Therefore, the polarization directions caused by the three magnetic configurations in Figs. 1(b)–1(d) are [001], [110], and [110], respectively. It should be noted that for cAFM1 and cAFM2 configurations, the initial magnetic moments shown in Fig. 1 are along the [$\bar{1}$10] axis, and the initial magnetic moment actually can be along other in-plane directions, such as the [110] axis. We test the polarization intensity and energy evolution with different initial in-plane magnetic moment, and find that they are the same. Similarly, for cAFM3, the in-plane magnetic field direction can also be along the [$\bar{1}$10] and [110] axis, again giving the same polarization and energy.

On the basis of the above three spin-canting configurations, we confirm the emergence of polarization in the case of spin canting. The effect of an applied magnetic field is simulated by fixing the direction of the magnetic moment [49]. We use α to indicate the angle between the spin moment and its initial direction. As shown in Figs. 1(e) and 1(f), when the α value

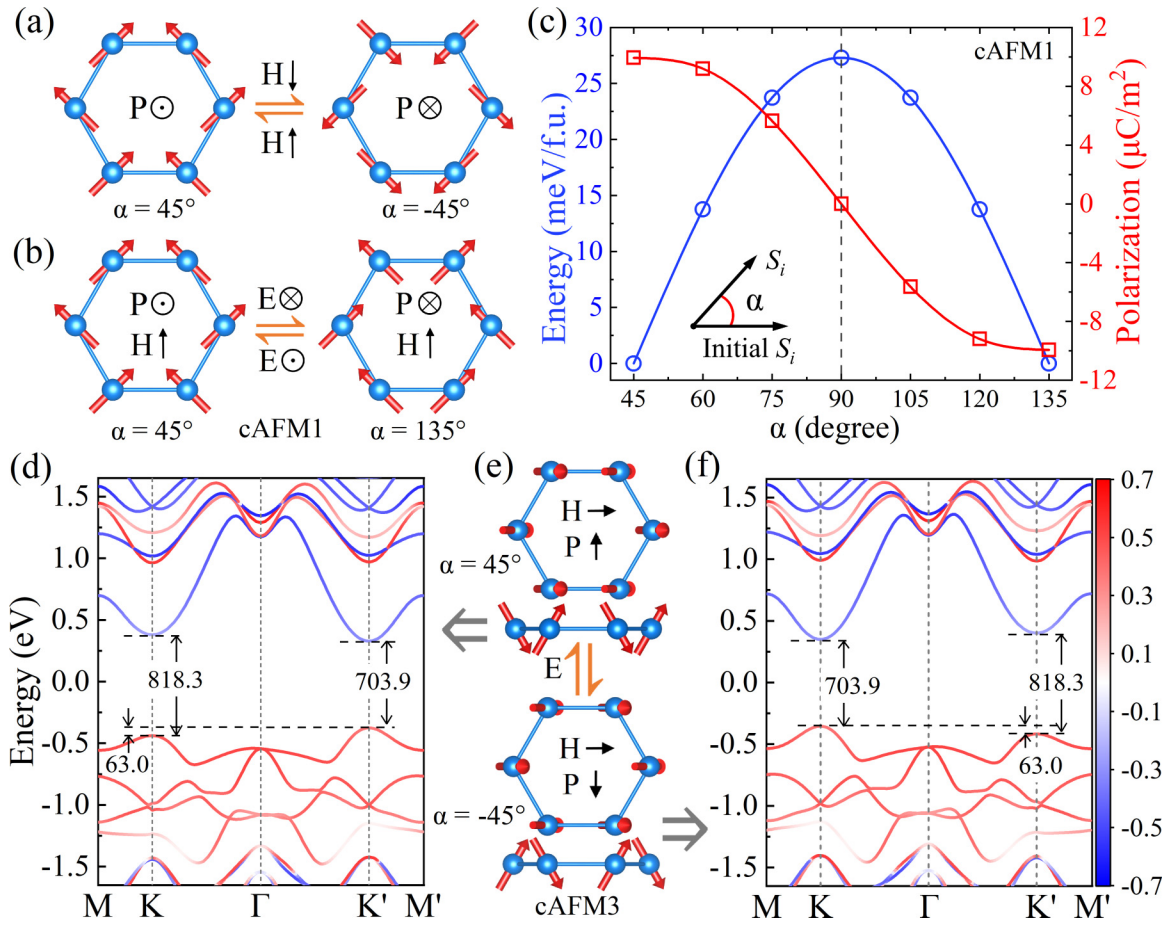

FIG. 2. (a) Ferroelectric polarization switching of cAFM1 configuration by magnetic field and (b) change of magnetic configuration by electric field, respectively. (c) Energy barrier and polarization evolution during ferroelectric switching from 45° to 135° cAFM1 configuration in the $MnPS_3$ monolayer. (d) Spin-resolved band structures and valley polarization for the $MnPSe_3$ monolayer under cAFM3 configurations with the deflection angle $\alpha = 45°$ and (f) $\alpha = -45°$, respectively. Red (blue) represents the spin projection in the positive (negative) direction of the magnetic field (spin up and spin down). (e) The schematic plot of magnetic structures, electric polarizations, and the intertransition of cAFM3 configurations with $\alpha = 45°$ and $-45°$.

increases, the electric polarization increases first then decreases, with the maximum polarization occurring around 45° with neighboring spins perpendicular to each other. Moreover, there is an obvious difference in the polarization intensity caused by the three spin-canting configurations. The maximum polarization of the $MnPS_3$ ($MnPSe_3$) monolayer is 9.94 (7.08), 29.22 (64.98), and 50.60 (58.55) $\mu C/m^2$ for cAFM1, cAFM2, and cAFM3 configurations, respectively. Simultaneously, during spin canting, the relative energy and total net magnetic moment also gradually increase with deflection angle from 0° to 90°, as shown in Fig. S5 in the Supplemental Material [24]. Above all, the spin canting induced by magnetic field can indeed drive the electric polarization of the hexagonal antiferromagnetic $MnPS_3$ ($MnPSe_3$) system. It should be pointed out that for simplicity, all the atoms are fixed at their collinear antiferromagnetic state during the calculations; thus the obtained electric polarization is purely electron contributed. In fact, the ions may show a significant response to magnetoelectricity in type-II multiferroics [50,51]. For our systems, test calculations show the polarization can be prominently improved with considering the ion displacement (Table S1 [24]). Thus, inclusion of the ion-displacement effect would facilitate obtaining a more realistic ferroelectric polarization.

Magnetoelectric and electric-valley coupling. The magnetoelectric coupling effect can intrinsically realize the control of ferroelectricity by magnetic field and in turn the control of magnetism by electric field, which is an important character for multiferroics [52]. Thus, for $MnPS_3$ ($MnPSe_3$) systems, it is necessary to study this dual regulation between electricity and magnetism. For the switching of electric polarization, since the polarization source is the cross-product part ($S_i \times S_j$) of the spin-canting configuration, reversing the direction of this product is a natural method. To achieve this purpose, an expected scheme is to change the applied magnetic field to the opposite direction. As shown in Fig. 2(a), when the direction of $S_i \times S_j$ is reversed by switching the magnetic field, the calculated polarization changes its sign, manifesting the control of ferroelectricity by magnetic field.

For the switching of magnetism, as shown in Fig. 2(b), under the condition of a fixed external magnetic field, there are two energy-degenerate spin-canting configurations, depending on $[1\bar{1}0]$ and $[\bar{1}10]$ initial magnetic moments, respectively.

Obviously, the electric polarization directions resulting from these two spin-canting situations are opposite. When an electric field is applied, there would be an energy difference between the two configurations, and the spin-canting configuration with polarization in the same direction as the electric field exhibits lower energy than the other. Moreover, the energy difference between the two spin-canting configurations increases with the applied electric field (Fig. S6 of the Supplemental Material [24]). Taking the 45° cAFM1 configuration of the $MnPS_3$ monolayer as an example, we calculate its spin-transition path when the deflection angle α changes from 45° to 135° [Fig. 2(c)]. It is clear that, along with spin transition, the electric polarization is completely reversed and the transition energy barrier is about 27.3 meV, which is even smaller than that of In_2Se_3 (66 meV) and $CuInP_2S_6$ (75 meV) [53,54]. Actually, a more realistic transition pathway would be cAFM1-cAFM3-cAFM1 (Fig. S7 [24]) by overcoming a significantly smaller energy barrier of about 22 μeV [24]. With such a barrier, we estimate that the electric field strength for switching the electric polarization of $MnPS_3$ and $MnPSe_3$ is around 0.1 and 0.5 V/Å, respectively. These results indicate that the electric field can switch the spin-driven polarization and change the spin configuration at the same time, realizing electric control of magnetism.

In addition to magnetoelectric coupling, we find that spin-canting also plays an important role in the electronic structure. Taking the cAFM3 configuration as an example, in the spin-resolved band structure and considering the spin-orbit-coupling effect, the valence band and conduction band exhibit opposite spin polarization along the direction of applied magnetic field (Figs. 2(d)–2(f) and Fig. S8 of the Supplemental Material [24]). This indicates that $MnPS_3$ and $MnPSe_3$ monolayers under the spin-canting configurations are excellent bipolar magnetic semiconductors. Based on bipolar magnetic semiconductors, completely spin-polarized currents with reversible spin polarization can be created and controlled simply by applying a gate voltage [7,55–61].

Furthermore, we discover significant valley polarization in the case of the cAFM3 configuration. As shown in Figs. 2(d)–2(f), the energy valleys at K and K' are obviously different with spin-orbital coupling included, and exhibit different band-gap values. The nonequivalent K/K' valleys are proved to enable the interband optical transitions obeying the valley-dependent selection rules with circularly polarized optical field by controlling the preferential occupation of carriers [62,63]. The spin-canting configuration simultaneously breaks the spatial and time inversion, which provides conditions for the emergence of valley polarization. Note that we find that cAFM1 and cAFM2 fail to exhibit valley polarization characteristic at any spin-canting angle. The corresponding band structures are shown in Fig. S8 of the Supplemental Material [24]. Besides, the $MnPSe_3$ monolayer can also exhibit valley polarization in the case of collinear antiferromagnetism with magnetic moment toward the [001] direction [64,65]. The dependence of the valence-band maximum difference at K and K' points, as well as the difference in band gap on deflection angle α, are calculated (Fig. S9 [24]), which indicate the size of valley polarization can be well tuned by the spin-canting angle. The maximum valley polarization occurs at approximately $\alpha = 45°$.

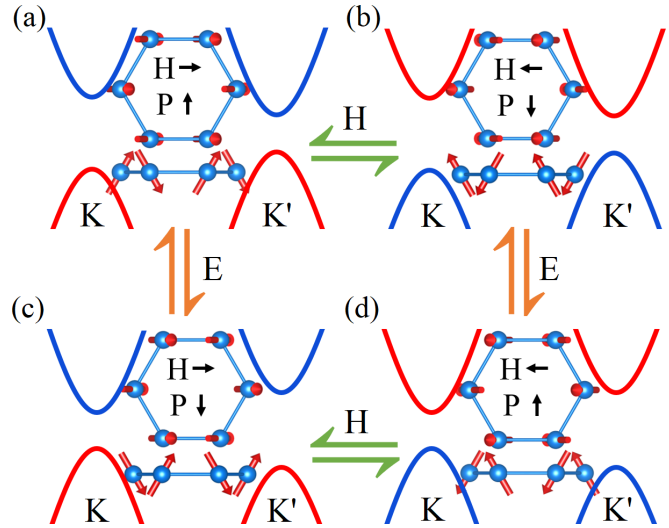

FIG. 3. [(a)–(d)] The illustration of electric and magnetic regulations of electric polarization, valley polarization, and magnetic texture. Spin-up and spin-down bands at K and K' valleys are denoted by red and blue curves, respectively.

Moreover, the valley polarization at K/K' can be reversed by an external electric field. As an example, in the cAFM3 configuration with deflection angle $\alpha = 45°$, the electric polarization is along the positive [110] direction. The valley at the K point is lower than the K' valley in energy level, establishing a valley polarization of 63.0 meV in the spin-up channel [Fig. 2(d)]. When the electric polarization is switched to the negative $[\bar{1}\bar{1}0]$ direction by an external electric field, the spin-deflection angle changes to $-45°$. It is notable that the K valley now becomes higher in energy than the K' valley, but the size of valley polarization in the spin-up channel is kept. Meanwhile, the direct band gap at the K point also changes from 818.3 meV to a smaller 703.9 meV. These features suggest that the switching of valley polarization can be controlled by switching the ferroelectric polarization.

Triple coupling of spin, electric, and valley. Moreover, based on the magnetoelectric coupling effect, we propose a potential scheme for mutual regulation of magnetism, ferroelectricity, and valley polarization by combining electric and magnetic fields, as shown in Fig. 3, which would facilitate the development of multifunctional applications [66–68]. In Fig. 3(a), the cAFM3 configuration caused by the magnetic field shows the bipolar magnetic semiconductor, electric polarization, and valley polarization properties. In the transition from Figs. 3(a) to 3(b), by reversing the direction of the magnetic field, the magnetic configuration is changed, resulting in the reversal of the spin-up and spin-down bands. Meanwhile, the spin-driven electric polarization is also switched because of magnetoelectric coupling. On the other hand, the transition from Figs. 3(a) to 3(c) illustrates the effect of an external electric field, the electric polarization opposite to the direction of the electric field is suppressed, and an asymmetry appears in spin-driven ferroelectric bistability, resulting in the reversal of the electric polarization and the corresponding change in the magnetic texture. Furthermore, the valley at the K/K' point follows the change of the magnetic configuration, causing

TABLE I. Symmetry operations relevant for the ferroelectric polarization parallel to the [001] direction in monolayer. The Y and N stand for inversion symmetry and inversion symmetry breaking, respectively, for each operation.

		m_z	S_3	S_6	i	C_{2x}	C_{2y}
Lattice	$P-3m1$	N	N	Y	Y	Y	N
Spin	Néel	Y	N	N	N	N	Y
	Zigzag	Y	N	N	Y	N	Y
	Stripe	Y	N	N	Y	N	N

the valence-band maximum originally located at the K' point to shift to the K point, which demonstrates the control of the valley polarization. Such effects of magnetic and electric fields also apply to the transitions from Figs. 3(c) to 3(d) and from Figs. 3(b) to 3(d). Therefore, the triple coupling is driven by the inherent magnetoelectric coupling in the spin-induced multiferroics, as well as the interaction of ferroelectricity and valley polarization.

Spin and lattice symmetry analysis. As is known, besides the Néel-type antiferromagnetic order such as in $MnPS_3$/$MnPSe_3$, the antiferromagnetism in a hexagonal lattice can also exhibit zigzag and stripe-type orders [69–71]. However, these two orders produce no electric polarization in spin-canting configurations. Thus, it is necessary to explore the underlying reasons for electric polarization and understand the spin-driven polarization differences between different antiferromagnetic orders. The basic requirement to drive ferroelectric polarization is to break the symmetry of space inversion, resulting in an asymmetry between positive and negative charge centers [72]. For spin-driven ferroelectric materials, we consider the crystal structure to be centrosymmetric, and the spin configuration helps break the space-inversion symmetry. Thus, analyzing the spin configuration from the perspective of symmetry is crucial to understanding the polarization mechanism. For example, in order to generate polarization in the out-of-plane [001] direction, the symmetry operations that need to be broken include mirror symmetry, rotation, reflection, and central inversion. We summarize six operations associated with out-of-plane polarization in Table I, including the mirror symmetry along the [001] direction (m_z), the threefold and sixfold rotation reflections (S_3 and S_6), the central inversion symmetry (i), and the double rotations along the in-plane symmetry axis (C_{2x} and C_{2y}). Taking the $MnPS_3$ monolayer (space group $P-3m1$) as an example, considering lattice symmetry first, the lattice only breaks three symmetry operations of m_z, S_3, and C_{2y}. Then, considering spin symmetry, the Néel-type spin-canting configuration breaks four symmetry operations (S_3, S_6, i, and C_{2x}), but fails to break the symmetry operations of m_z and C_{2y}. Finally, combining the lattice symmetry and spin symmetry, the six symmetry operations associated with z-direction polarization are all broken. On the contrary, for zigzag and stripe orders, neither the lattice nor the spin-canting configuration breaks the central inversion symmetry, as shown in Fig. S10 of the Supplemental Material [24]. These results indicate that the occurring of magnetopolarization under spin canting requires not only a special spin configuration but also a specific lattice symmetry.

In summary, based on first-principles calculations, spin canting under an external magnetic field is demonstrated as a potential route to endow the 2D hexagonal antiferromagnetic semiconductors $MnPS_3$ and $MnPSe_3$ with triple coupling of spin, electric, and valley polarization. Furthermore, a symmetry analysis scheme combining the symmetries of both lattice and spin is suggested to achieve spin-canting-driven multiferroics in more antiferromagnetic systems. This work aims to provide a feasible scheme that can effectively promote the solution to the lack of magnetoelectric coupling in antiferromagnetic semiconductor materials, and explore interaction of various physical properties.

Acknowledgments. This work was supported by the National Natural Science Foundation of China (Grants No. 22288201, No. 22273092, and No. 22322304), by the Innovation Program for Quantum Science and Technology (Grant No. 2021ZD0303306), by the Strategic Priority Research Program of the Chinese Academy of Sciences (Grant No. XDB0450101), by the project funded by the China Postdoctoral Science Foundation with Grants No. 2024M753079 and No. 2024T170873, by USTC Tang Scholar, and by the Postdoctoral Fellowship Program of CPSF.

[1] M. B. Jungfleisch, W. Zhang, and A. Hoffmann, Perspectives of antiferromagnetic spintronics, Phys. Lett. A **382**, 865 (2018).

[2] C. Gong, P. Y. Zhang, T. Norden, Q. W. Li, Z. Guo, A. Chaturvedi, A. Najafi, S. F. Lan, X. Z. Liu, Y. Wang, S. J. Gong, H. Zeng, H. Zhang, A. Petrou, and X. Zhang, Ferromagnetism emerged from non-ferromagnetic atomic crystals, Nat. Commun. **14**, 3839 (2023).

[3] T. Jungwirth, X. Marti, P. Wadley, and J. Wunderlich, Antiferromagnetic spintronics, Nat. Nanotechnol. **11**, 231 (2016).

[4] H. Yan, Z. X. Feng, P. X. Qin, X. R. Zhou, H. X. Guo, X. N. Wang, H. Y. Chen, X. Zhang, H. J. Wu, C. B. Jiang, and Z. Q. Liu, Electric-field-controlled antiferromagnetic spintronic devices, Adv. Mater. **32**, 1905603 (2020).

[5] V. Baltz, A. Manchon, M. Tsoi, T. Moriyama, T. Ono, and Y. Tserkovnyak, Antiferromagnetic spintronics, Rev. Mod. Phys. **90**, 015005 (2018).

[6] S. Rahman, J. F. Torres, A. R. Khan, and Y. R. Lu, Recent developments in van der Waals antiferromagnetic 2D materials: Synthesis, characterization, and device implementation, ACS Nano **15**, 17175 (2021).

[7] X. X. Li and J. L. Yang, First-principles design of spintronics materials, Natl. Sci. Rev. **3**, 365 (2016).

[8] J. H. Han, R. Cheng, L. Q. Liu, H. Ohno, and S. Fukami, Coherent antiferromagnetic spintronics, Nat. Mater. **22**, 684 (2023).

[9] W. Sun, W. X. Wang, J. D. Zang, H. Li, G. B. A. Zhang, J. L. Wang, and Z. X. Cheng, Manipulation of magnetic skyrmion in a 2D van der Waals heterostructure via both electric and magnetic fields, Adv. Funct. Mater. **31**, 2104452 (2021).

[10] A. Haykal, J. Fischer, W. Akhtar, J. Y. Chauleau, D. Sando, A. Finco, F. Godel, Y. A. Birkholzer, C. Carretero, N. Jaouen, M. Bibes, M. Viret, S. Fusil, V. Jacques, and V. Garcia,

Antiferromagnetic textures in $BiFeO_3$ controlled by strain and electric field, Nat. Commun. **11**, 1704 (2020).

[11] P. X. Zhang, C. T. Chou, H. H. Yun, B. C. McGoldrick, J. T. Hou, K. A. Mkhoyan, and L. Q. Liu, Control of Néel vector with spin-orbit torques in an antiferromagnetic insulator with tilted easy plane, Phys. Rev. Lett. **129**, 017203 (2022).

[12] T. X. Li, S. W. Jiang, N. Sivadas, Z. F. Wang, Y. Xu, D. Weber, J. E. Goldberger, K. Watanabe, T. Taniguchi, C. J. Fennie, K. F. Mak, and J. Shan, Pressure-controlled interlayer magnetism in atomically thin CrI_3, Nat. Mater. **18**, 1303 (2019).

[13] H. H. Kim, B. W. Yang, S. W. Li, S. W. Jiang, C. H. Jin, Z. Tao, G. Nichols, F. Sfigakis, S. Z. Zhong, C. H. Li, S. J. Tian, D. G. Cory, G. X. Miao, J. Shan, K. F. Mak, H. C. Lei, K. Sun, L. Y. Zhao, and A. W. Tsen, Evolution of interlayer and intralayer magnetism in three atomically thin chromium trihalides, Proc. Natl. Acad. Sci. USA **116**, 11131 (2019).

[14] S. O. Valenzuela and S. Roche, The phase diagram of 2D antiferromagnets, Nat. Nanotechnol. **14**, 1088 (2019).

[15] D. R. Klein, D. MacNeill, Q. Song, D. T. Larson, S. A. Fang, M. Y. Xu, R. A. Ribeiro, P. C. Canfield, E. Kaxiras, R. Comin, and P. Jarillo-Herrero, Enhancement of interlayer exchange in an ultrathin two-dimensional magnet, Nat. Phys. **15**, 1255 (2019).

[16] Z. Wang, M. Gibertini, D. Dumcenco, T. Taniguchi, K. Watanabe, E. Giannini, and A. F. Morpurgo, Determining the phase diagram of atomically thin layered antiferromagnet $CrCl_3$, Nat. Nanotechnol. **14**, 1116 (2019).

[17] T. Kimura, T. Goto, H. Shintani, K. Ishizaka, T. Arima, and Y. Tokura, Magnetic control of ferroelectric polarization, Nature (London) **426**, 55 (2003).

[18] H. Mitamura, R. Watanuki, K. Kaneko, N. Onozaki, Y. Amou, S. Kittaka, R. Kobayashi, Y. Shimura, I. Yamamoto, K. Suzuki, S. Chi, and T. Sakakibara, Spin-chirality-driven ferroelectricity on a perfect triangular lattice antiferromagnet, Phys. Rev. Lett. **113**, 147202 (2014).

[19] J. J. Zhang, L. F. Lin, Y. Zhang, M. H. Wu, B. I. Yakobson, and S. Dong, Type-II multiferroic $Hf_2VC_2F_2$ MXene monolayer with high transition temperature, J. Am. Chem. Soc. **140**, 9768 (2018).

[20] Q. Song, C. A. Occhialini, E. Ergecen, B. Ilyas, D. Amoroso, P. Barone, J. Kapeghian, K. Watanabe, T. Taniguchi, A. S. Botana, S. Picozzi, N. Gedik, and R. Comin, Evidence for a single-layer van der Waals multiferroic, Nature (London) **602**, 601 (2022).

[21] J. T. Zhang, Y. Zhou, F. Wang, X. F. Shen, J. L. Wang, and X. M. Lu, Coexistence and coupling of spin-induced ferroelectricity and ferromagnetism in perovskites, Phys. Rev. Lett. **129**, 117603 (2022).

[22] Y. J. Sun, Q. H. Tan, X. L. Liu, Y. F. Gao, and J. Zhang, Probing the magnetic ordering of antiferromagnetic $MnPS_3$ by Raman spectroscopy, J. Phys. Chem. Lett. **10**, 3087 (2019).

[23] N. Sivadas, M. W. Daniels, R. H. Swendsen, S. Okamoto, and D. Xiao, Magnetic ground state of semiconducting transition-metal trichalcogenide monolayers, Phys. Rev. B **91**, 235425 (2015).

[24] See Supplemental Material at http://link.aps.org/supplemental/10.1103/PhysRevB.110.094409 for spin-canting energy and polarization evolution, energy barrier and net magnetic moment, the effect of electric field, spin-resolved band structure, band-gap evolution, spin-canting models for other antiferromagnetic orders, and ferroelectric polarization considering ion displacement, which includes Refs. [25–45].

[25] J. Sodequist and T. Olsen, Type II multiferroic order in two-dimensional transition metal halides from first principles spin-spiral calculations, 2D Mater. **10**, 035016 (2023).

[26] G. Kresse and J. Furthmüller, Efficiency of *ab-initio* total energy calculations for metals and semiconductors using a plane-wave basis set, Comput. Mater. Sci. **6**, 15 (1996).

[27] H. J. Xiang, C. Lee, H. J. Koo, X. G. Gong, and M. H. Whangbo, Magnetic properties and energy-mapping analysis, Dalton Trans. **42**, 823 (2013).

[28] R. Resta, Theory of the electric polarization in crystals, Ferroelectrics **136**, 51 (1992).

[29] J. R. Miller, The NHMFL 45-T hybrid magnet system: Past, present, and future, IEEE Trans. Appl. Supercond. **13**, 1385 (2003).

[30] F. Lou, X. Y. Li, J. Y. Ji, H. Y. Yu, J. S. Feng, X. G. Gong, and H. J. Xiang, PASP: Property analysis and simulation package for materials, J. Chem. Phys. **154**, 114103 (2021).

[31] S. Grimme, Semiempirical GGA-type density functional constructed with a long-range dispersion correction, J. Comput. Chem. **27**, 1787 (2006).

[32] N. Vonrüti and U. Aschauer, Band-gap engineering in $AB(O_xS_{1-x})_3$ perovskite oxysulfides: A route to strongly polar materials for photocatalytic water splitting, J. Mater. Chem. A **7**, 15741 (2019).

[33] S. Hahn, K. Kim, K. Kim, X. B. Hu, T. Painter, I. Dixon, S. Kim, K. R. Bhattarai, S. Noguchi, J. Jaroszynski, and D. C. Larbalestier, 45.5-tesla direct-current magnetic field generated with a high-temperature superconducting magnet, Nature (London) **570**, 496 (2019).

[34] Y. B. Zhang, T. T. Tang, C. Girit, Z. Hao, M. C. Martin, A. Zettl, M. F. Crommie, Y. R. Shen, and F. Wang, Direct observation of a widely tunable bandgap in bilayer graphene, Nature (London) **459**, 820 (2009).

[35] D. Maryenko, A. McCollam, J. Falson, Y. Kozuka, J. Bruin, U. Zeitler, and M. Kawasaki, Composite fermion liquid to Wigner solid transition in the lowest Landau level of zinc oxide, Nat. Commun. **9**, 4356 (2018).

[36] S. P. Beckman, X. J. Wang, K. M. Rabe, and D. Vanderbilt, Ideal barriers to polarization reversal and domain-wall motion in strained ferroelectric thin films, Phys. Rev. B **79**, 144124 (2009).

[37] P. E. Blöchl, Projector augmented-wave method, Phys. Rev. B **50**, 17953 (1994).

[38] E. Bousquet and N. Spaldin, J dependence in the LSDA + U treatment of noncollinear magnets, Phys. Rev. B **82**, 220402(R) (2010).

[39] R. D. King-Smith and D. Vanderbilt, Theory of polarization of crystalline solids, Phys. Rev. B **47**, 1651 (1993).

[40] G. Kresse and J. Furthmüller, Efficient iterative schemes for *ab initio* total-energy calculations using a plane-wave basis set, Phys. Rev. B **54**, 11169 (1996).

[41] G. Kresse and D. Joubert, From ultrasoft pseudopotentials to the projector augmented-wave method, Phys. Rev. B **59**, 1758 (1999).

[42] A. I. Liechtenstein, V. I. Anisimov, and J. Zaanen, Density-functional theory and strong-interactions: Orbital ordering in Mott-Hubbard insulators, Phys. Rev. B **52**, R5467(R) (1995).

[43] L. Wang, T. Maxisch, and G. Ceder, Oxidation energies of transition metal oxides within the GGA+U framework, Phys. Rev. B **73**, 195107 (2006).

[44] J. P. Perdew, K. Burke, and M. Ernzerhof, Generalized gradient approximation made simple, Phys. Rev. Lett. **77**, 3865 (1996).
[45] J. Stein, S. Biesenkamp, T. Cronert, T. Fröhlich, J. Leist, K. Schmalzl, A. C. Komarek, and M. Braden, Combined Arrhenius-Merz law describing domain relaxation in type-II multiferroics, Phys. Rev. Lett. **127**, 097601 (2021).
[46] H. J. Xiang, E. J. Kan, Y. Zhang, M. H. Whangbo, and X. G. Gong, General theory for the ferroelectric polarization induced by spin-spiral order, Phys. Rev. Lett. **107**, 157202 (2011).
[47] H. Katsura, N. Nagaosa, and A. V. Balatsky, Spin current and magnetoelectric effect in noncollinear magnets, Phys. Rev. Lett. **95**, 057205 (2005).
[48] S. Miyahara and N. Furukawa, Theory of antisymmetric spin-pair-dependent electric polarization in multiferroics, Phys. Rev. B **93**, 014445 (2016).
[49] P. W. Ma and S. L. Dudarev, Constrained density functional for noncollinear magnetism, Phys. Rev. B **91**, 054420 (2015).
[50] A. Malashevich and D. Vanderbilt, First principles study of improper ferroelectricity in $TbMnO_3$, Phys. Rev. Lett. **101**, 037210 (2008).
[51] I. A. Sergienko and E. Dagotto, Role of the Dzyaloshinskii-Moriya interaction in multiferroic perovskites, Phys. Rev. B **73**, 094434 (2006).
[52] G. Lawes and G. Srinivasan, Introduction to magnetoelectric coupling and multiferroic films, J. Phys. D: Appl. Phys. **44**, 243001 (2011).
[53] W. J. Ding, J. B. Zhu, Z. Wang, Y. F. Gao, D. Xiao, Y. Gu, Z. Y. Zhang, and W. G. Zhu, Prediction of intrinsic two-dimensional ferroelectrics in InSe and other III-VI van der Waals materials, Nat. Commun. **8**, 14956 (2017).
[54] S. N. Neal, S. Singh, X. C. Fang, C. Won, F. T. Huang, S. W. Cheong, K. M. Rabe, D. Vanderbilt, and J. L. Musfeldt, Vibrational properties of CuInPS across the ferroelectric transition, Phys. Rev. B **105**, 075151 (2022).
[55] X. X. Li, X. J. Wu, Z. Y. Li, J. L. Yang, and J. G. Hou, Bipolar magnetic semiconductors: A new class of spintronics materials, Nanoscale **4**, 5680 (2012).
[56] X. X. Li, X. J. Wu, and J. L. Yang, Half-metallicity in $MnPSe_3$ exfoliated nanosheet with carrier doping, J. Am. Chem. Soc. **136**, 11065 (2014).
[57] H. D. Wang, Q. Q. Feng, X. X. Li, and J. L. Yang, High-throughput computational screening for bipolar magnetic semiconductors, Research (Washington, DC, US) **2022**, 9857631 (2022).
[58] J. Y. Li, X. X. Li, and J. L. Yang, A review of bipolar magnetic semiconductors from theoretical aspects, Fundam. Res. **2**, 511 (2022).
[59] Y. J. Hu, X. X. Li, Q. X. Li, and J. L. Yang, Bipolar magnetic molecules for spin-polarized electric current in molecular junctions, Angew. Chem. Int. Ed. **61**, e202205036 (2022).
[60] X. Y. Li, Q. B. Liu, Y. S. Tang, W. Li, N. Ding, Z. Liu, H. H. Fu, S. Dong, X. X. Li, and J. L. Yang, Quintuple function integration in two-dimensional Cr(II) five-membered heterocyclic metal organic frameworks via tuning ligand spin and lattice symmetry, J. Am. Chem. Soc. **145**, 7869 (2023).
[61] J. Y. Li, X. X. Li, and J. L. Yang, Chemically controlled reversible magnetic phase transition in two-dimensional organometallic lattices, Nano Lett. **23**, 9126 (2023).
[62] T. Hu, G. D. Zhao, H. Gao, Y. B. Wu, J. S. Hong, A. Stroppa, and W. Ren, Manipulation of valley pseudospin in WSe_2/CrI_3 heterostructures by the magnetic proximity effect, Phys. Rev. B **101**, 125401 (2020).
[63] D. Xiao, G. B. Liu, W. X. Feng, X. D. Xu, and W. Yao, Coupled spin and valley physics in monolayers of MoS_2 and other group-VI dichalcogenides, Phys. Rev. Lett. **108**, 196802 (2012).
[64] Q. Pei and W. Mi, Electrical control of magnetic behavior and valley polarization of monolayer antiferromagnetic $MnPSe_3$ on an insulating ferroelectric substrate from first principles, Phys. Rev. Appl. **11**, 014011 (2019).
[65] Q. Q. Xue, X. C. Mu, Y. Sun, and J. Zhou, Valley contrasting bulk photovoltaic effect in a *PT*-symmetric $MnPSe_3$ monolayer, Phys. Rev. B **107**, 245404 (2023).
[66] Y. Z. Wu, J. W. Tong, L. Deng, F. F. Luo, F. B. Tian, G. W. Qin, and X. M. Zhang, Coexisting ferroelectric and ferrovalley polarizations in bilayer stacked magnetic semiconductors, Nano Lett. **23**, 6226 (2023).
[67] J. X. Li, W. Q. Li, S. H. Hung, P. L. Chen, Y. C. Yang, T. Y. Chang, P. W. Chiu, H. T. Jeng, and C. H. Liu, Electric control of valley polarization in monolayer WSe_2 using a van der Waals magnet, Nat. Nanotechnol. **17**, 721 (2022).
[68] Y.-Q. Li, X. Zhang, X. Shang, Q.-W. He, D.-S. Tang, X.-C. Wang, and C.-G. Duan, Magnetic and ferroelectric manipulation of valley physics in Janus piezoelectric materials, Nano Lett. **23**, 10013 (2023).
[69] J. U. Lee, S. Lee, J. H. Ryoo, S. Kang, T. Y. Kim, P. Kim, C. H. Park, J. G. Park, and H. Cheong, Ising-type magnetic ordering in atomically thin $FePS_3$, Nano Lett. **16**, 7433 (2016).
[70] M. J. Coak, D. M. Jarvis, H. Hamidov, A. R. Wildes, J. A. M. Paddison, C. Liu, C. R. S. Haines, N. T. Dang, S. E. Kichanov, B. N. Savenko, S. Lee, M. Kratochvilova, S. Klotz, T. C. Hansen, D. P. Kozlenko, J. G. Park, and S. S. Saxena, Emergent magnetic phases in pressure-tuned van der Waals antiferromagnet $FePS_3$, Phys. Rev. X **11**, 011024 (2021).
[71] S. Y. Kim, T. Y. Kim, L. J. Sandilands, S. Sinn, M. C. Lee, J. Son, S. Lee, K. Y. Choi, W. Kim, B. G. Park, C. Jeon, H. D. Kim, C. H. Park, J. G. Park, S. J. Moon, and T. W. Noh, Charge-spin correlation in van der Waals antiferromagnet $NiPS_3$, Phys. Rev. Lett. **120**, 136402 (2018).
[72] N. A. Spaldin, A beginner's guide to the modern theory of polarization, J. Solid State Chem. **195**, 2 (2012).